Smart Structures and Systems, *Vol. 36, No. 2 (2025) 123-137*
https://doi.org/10.12989/sss.2025.36.2.123

A hybrid RNN-fuzzy-PSO model for forecasting multiple transverse cracks in laminated composite beam-like structures

Sarada Prasad Parida [1], Saritprava Sahoo [2] and Pankaj Charan Jena[*2]

[1] *Konark Institute of Science & Technology, Mechanical Engineering, Bhubaneswar, Odisha, India*
[2] *VSS University of Technology, Production Engineering, Burla, Odisha, India*

(*Received May 22, 2025, Revised August 18, 2025, Accepted August 20, 2025*)

Abstract. This study investigates the use of a hybrid artificial intelligence (AI) model combining Recurrent Neural Networks (RNN), Fuzzy Inference (FI), and Particle Swarm Optimization (PSO) for predicting the position and severity of multiple transverse cracks in glass-fiber-reinforced-laminated-composite (GFLCB) beams. To assess the model's accuracy, a verification was conducted using a GFLCB intact and a double cracked beam. Finite Element Analysis (FEA) was employed to determine the first three relative natural frequencies (RNFs) under double crack conditions. Then the obtained RNFs are used to train the programs to locate the crack location and depth. The supremacy of the model over mPSO, RNN, and RNN-mPSO is verified. The maximum error percentage in calculation of first crack location by RNN-FUZZY-PSO, mPSO, RNN, and RNN-mPSO is found to be 3.08%, 5%, 7.2%, and 8.11% respectively. While in detection of crack locations, the error percentage are 1.1%, 5%, 7.2%, and 8.11%, respectively. Further RNN-FUZZY-PSO is used to diagnose the crack severity and locations of multiple cracks (nine crack) in hybrid GFLCB. Results indicated that the RNFs are significantly influenced by the number and severity of the cracks. The predicted crack positions and severities by the method are with a marginal error of 1.53% and 1.3%, respectively. The model shows improved accuracy as the number of cracks increased, especially for the ninth crack, where the mean square error is 0.01154, with maximum error percentage of 0.8%. The findings demonstrate the proposed AI model's effectiveness for precise identification of crack positions and severities in GFLCB structures with multiple cracks.

Keywords: finite element analysis; laminated composite; RNN-Fuzzy-PSO model; severity; transverse-multi-cracks

1. Introduction

The strength of Laminated Composite Beams (LCBs) in various engineering applications largely depends on their fiber orientation and material properties (Duan *et al*. 2020). The choice of natural organic fillers not only improve the required strength but also improves environmental sustainability and agricultural waste management though preparation of these polymer based composites needs special care (Davim 2017a). It is very much important to choose the suitable design and fabrication method to get the optimized strength at a cost effective manner. In this regard, some of the useful statistical techniques are discussed (Davim 2017b). The occurrence of cracks is inevitable due to geometric constraints and various loading conditions, such as buckling (Kaveh *et al*. 2019). Similarly, drilling in laminated composites causes delamination though delamina-tion factor can be accessed numerically and its effect can be investigated (Davim *et al*. 2007). Early crack detection is critical, as undetected damage can escalate into catastrophic failure. Among the methods used for damage detection, vibration-based techniques are widely applied, utilizing frequency response functions to detect damage and assess sensitivity in beam structures (Dos Santos *et al*. 2005, Capozucca and Magagnini 2018). Additionally, acceleration analysis can be used to predict structural faults (Nikkhoo *et al*. 2021). Another effective method for fault identification in composite structures is wavelet transform method (Zhou *et al*. 2018), which has also been employed to detect issues in rotor system bearings (Sun *et al*. 2013).

Several studies have explored different techniques for rapid damage detection in composite materials. For example, Khatir *et al*. (2018) proposed a method for quick damage detection in Carbon Fiber Reinforced Polymer (CFRP) composites using the Finite Element Method (FEM) and experimental data. Liu *et al*. (2022) developed a 3D FE model to simulate breathing cracks in rotor systems and examine the effects of crack positions. Similarly, Sepehry *et al*. (2021) demonstrated that the scaled boundary-FEM is a promising technique for identifying breathing cracks in structures. FEM has also been identified as an ideal optimization approach for quickly locating and assessing damage (Gomes *et al*. 2019).

In recent years, AI techniques, especially reverse-engineering methods, have gained attention for damage detection in composite structures. Zang and Imregun (2001) utilized frequency data as input for Artificial Neural Networks (ANN) to identify structural damage. Abdeljaber *et al*. (2017) introduced Convolutional Neural Networks

*Corresponding author, Ph.D., Associate Professor,
E-mail: pcjena_pe@vssut.ac.in
[a] Ph.D., Associate Professor,
E-mail: sarada800@gmail.com
[b] Ph.D., E-mail: saritprava@gmail.com

ISSN: 1738-1584 (Print), 1738-1991 (Online)

(CNN) to detect deterioration in large-scale steel frames. Babu Rao and Mallikarjuna Reddy (2021) used ANN to predict potential cracks and depths in rotor systems with 99.19% accuracy. Gomes *et al*. (2019) combined ANN with Genetic Algorithms (GA) to detect delamination in laminated composite plates. Additionally, deep learning models combining CNN and Recurrent Neural Networks (RNN) have been developed for crack location detection in isotropic beam structures (Rautela and Gopalakrishnan 2020).

Fuzzy logic techniques have also been applied to structural damage detection. Zadeh's (1965) fuzzy technique has been used to address structural damage, with rule-based systems employed to mitigate noise in rotor blade (Ganguli 2001). Fuzzy Inference Systems (FIS) have been used to determine crack parameters in cantilever beams (Dash 2013, Thatoi *et al*. 2014, Chandrashekhar and Ganguli 2009). More recently, hybridized FIS models have been used to detect crack locations and depths in composite beams based on shifts in vibration modes (Das *et al*. 2021, Das *et al*. 2024). These models provide accurate predictions, closely matching experimental results.

The Adaptive Neuro-Fuzzy Inference System (ANFIS), introduced by Jang (1993), has been applied in various fields, including fire-induced spalling prediction (Seitllari and Naser 2019) and shear strength assessment (Naderpour and Mirrashid 2018). Meanwhile, Particle Swarm Optimization (PSO) methods have gained popularity for accurately retrieving unknown parameters. PSO with dynamic inertia weight has been used to analyze beam flexibility (Mohamad *et al*. 2009). Kang *et al*. (2012) developed an immunity-enhanced PSO to provide optimal and accurate damage assessments, and Nouri Shirazi *et al*. (2014) used a modified PSO for identifying failures in isotropic structures. Other studies have integrated PSO with ANFIS to predict critical buckling in circular steel beams (Nguyen *et al*. 2020) and used RNN-PSO to detect crack locations in cantilever beams (Parida *et al*. 2024). Additionally, Sahoo and Jena (2021a) employed ANN for detecting single crack locations and depths in composite beams. These advancements indicate that a combination of AI techniques, FEM, and optimization methods can significantly enhance the accuracy and efficiency of damage detection in composite structures, offering promising solutions for the integrity monitoring of engineering systems.

Although several quantitative crack diagnostic methods, such as Fuzzy Logic, Genetic Algorithms (GA), Artificial Neural Networks (ANN), Recurrent Neural Networks (RNN), and Particle Swarm Optimization (PSO), are well-documented in the literature, the use of hybrid models remain underdeveloped, particularly in addressing multi-crack parameters in anisotropic composite structures. This gap in research presents an opportunity for developing novel hybrid AI techniques to tackle these challenges. The primary goal of the current study is to design such a hybrid tool specifically aimed at addressing multi-crack parameters in glass-fiber-reinforced-laminated-composite beams (GFLCB). To achieve this, the study proposes a hybrid model that combines RNN with fuzzy logic and modified PSO (mPSO) for identifying crack locations and their severities. This integrated approach is formulated as a reverse technique that utilizes dynamic excitation. In this context, Finite Element Analysis (FEA) is employed to determine the three relative natural frequencies of the structure, which are then optimized and used as input data for the RNN-Fuzzy-mPSO model implemented in MATLAB. The results reveal that this hybrid RNN-Fuzzy-mPSO model minimizes the mean absolute percentage error in damage assessment, demonstrating its effectiveness in accurately predicting multiple crack locations and depths.

2. Analytical model

For the current study, a polyester-glass GFLCB (cantilever) with multiple transverse cracks as shown in Fig. 1(a) is considered. The mechanical properties of GFLCB are considered using mixture rule (Sahoo and Jena 2021b). The modal characteristics are then incorporated by Castigliano's theorem where the natural frequency and mode-shape are considered as the function of strain-energy release rate. It is assumed that, due to the presence of cracks, the stiffness value is changed, and this is due to an additional increase in local flexibility.

Assuming the GFLCB with 'n' number of cracks, The local-flexibility at n^{th} crack site as a function of strain energy release rate is given by Dash (2013)

$$\left(C_{ij}\right)_n = \frac{\partial^2}{\partial P_1 \partial P_2}\int_0^W \int_0^{a_n} J(\beta)_n \, d\beta dH \qquad i,j = 1,2 \tag{1}$$

Where P_1, and P_2 are the axial and bending loads applied to the LHCB. 'W' denotes width of beam and 'a_n' denotes height of the nth crack. The strain energy release rate for nth crack is given by

$$J(\beta)_n = \frac{1-\nu^2}{E}\left[\sum_{n=1}^{3}(K_{In})^2 + (K_{IIn})^2 + (K_{IIIn})^2\right] \tag{2}$$

With

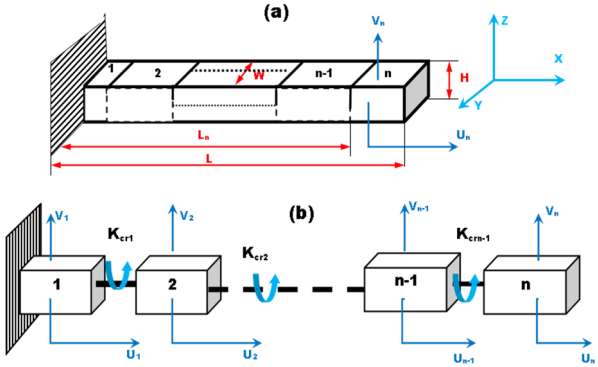

Fig. 1 Schematic diagram of beam: (a) GFRPLCB with multiple transverse crack; (b) equivalent spring model

$$\beta_n = \frac{a_n}{H}$$

The stress intensity factors for axial and bending loads P_1 and P_2 is given by

$$K_{In} = \frac{P_1}{WH}\sqrt{\pi\beta_n F_I\left(\frac{\beta_n}{H}\right)} \tag{3a}$$

$$K_{IIn} = \frac{6P_2}{WH^2}\sqrt{\pi\beta_n F_{II}\left(\frac{\beta_n}{H}\right)} \tag{3b}$$

$$K_{IIn} = 0 \tag{3c}$$

Where

$$F_I\left(\frac{\beta_n}{H}\right) = \frac{1.122 - 0.561(\chi_n) + 0.085(\chi_n)^2 + 0.18(\chi_n)^3}{\sqrt{1-(\chi_n)}} \tag{4}$$

$$F_{II}\left(\frac{\beta_n}{H}\right) = \sqrt{\frac{tan\,\chi_n}{\chi_n}}\frac{[0.923 + 0.199(1 - sin(\chi_n))^4]}{cos(\chi_n)} \tag{5}$$

With

$$\chi_n = \frac{\pi\beta_n}{2H}$$

The stiffness of the GFLCB in relation to overall stiffness can be represented as Dash (2013)

$$C_{ij} = \sum_{m=1}^{n}(C_{ij})_m = \sum_{m=1}^{n}\left(\frac{\partial U_{ij}}{\partial P_2}\right) = \frac{\partial^2}{\partial P_1 \partial P_2}\int_0^W\int_0^{a_m} J(\beta)_m d\beta dH \tag{6}$$
$$i,j = 1,2 \text{ and } m = 1{:}n$$

$$K_{Cr} = C_{ij}^{-1} = \left[\frac{\partial^2}{\partial P_1 \partial P_2}\int_0^W\int_0^{a_n} J(\beta)_n d\beta dH\right]^{-1} \tag{7}$$

The strain energy in GFLCB following Castigliano's expression for displacement is given by Krawczuk and Ostachowicz 1995)

$$\Gamma = \sum_{i=1}^{2}\frac{\partial U}{\partial P_i} = \sum_{i=1}^{2}\frac{\partial}{\partial P_i}\left(\frac{P_i^2 L^3}{96EI} + \frac{P_i^2 {\zeta_n}^2}{8K_{eff}}\right) \tag{8}$$

Where

$$\zeta_n = \frac{L_e}{L}, \qquad L_e = L_n - L_{n-1}$$

Ln: length of nth cracked beam segment and L: length of the LHCB. Now the Eigen values of frequencies from the characteristic's equation as

$$\left[(K_{Eff})^2 - \omega^2 M_{eff}\right]\psi = 0 \tag{9}$$

The stiffness and mass matrix of the GFLCB with 'n' number of crack can be derived by considering it as 'n+1' beam segments attached by rotational springs as shown in Fig. 1(b). Considering the length of cracked beam portion as 'L_e', width 'W', height 'H_e', and height of crack 'a_n'; the elemental mass and stiffness matrix $[M_e]$ and $[K_e]$ for each cracked beam segment can be derived according to the position and height of each crack. Further individual mass and stiffness matrices are assembled to get global mass and stiffness matrix. The elemental mass and stiffness matrix $[M_e]$ and $[K_e]$ for each cracked beam segment are given by (Krawczuk and Ostachowicz 1995, Jena *et al*. 2017)

$$[M] = \rho_c B_e H_e L_e \begin{bmatrix}
\frac{2}{15} & 0 & 0 & \frac{2}{15} & 0 & 0 & \frac{-1}{30} & 0 & 0 \\
0 & \frac{2}{15} & \frac{L_e}{180} & 0 & \frac{1}{15} & \frac{-L_e}{90} & 0 & \frac{-1}{30} & \frac{L_e}{180} \\
0 & \frac{L_e}{180} & \frac{{L_e}^2}{1890}+\frac{{H_e}^2}{90} & 0 & 0 & \frac{-{L_e}^2}{945}+\frac{{H_e}^2}{180} & 0 & \frac{-L_e}{180} & \frac{{L_e}^2}{1890}-\frac{{H_e}^2}{360} \\
\frac{2}{15} & 0 & 0 & \frac{8}{15} & 0 & 0 & \frac{1}{15} & 0 & 0 \\
0 & \frac{1}{15} & 0 & 0 & \frac{8}{15} & 0 & 0 & \frac{1}{15} & 0 \\
0 & \frac{-L_e}{90} & \frac{-{L_e}^2}{945}+\frac{{H_e}^2}{180} & 0 & 0 & \frac{2{L_e}^2}{945}+\frac{{H_e}^2}{180} & 0 & \frac{L_e}{90} & \frac{-{L_e}^2}{945}+\frac{{H_e}^2}{180} \\
\frac{-1}{30} & 0 & 0 & \frac{1}{15} & 0 & 0 & \frac{2}{15} & 0 & 0 \\
0 & \frac{-1}{30} & \frac{-L_e}{180} & 0 & \frac{1}{15} & \frac{L_e}{90} & 0 & \frac{2}{15} & \frac{-L_e}{180} \\
0 & \frac{L_e}{180} & \frac{{L_e}^2}{1890}-\frac{{H_e}^2}{90} & 0 & 0 & \frac{-{L_e}^2}{945}+\frac{{H_e}^2}{180} & 0 & \frac{-L_e}{180} & \frac{{L_e}^2}{1890}+\frac{{H_e}^2}{90}
\end{bmatrix} \tag{10}$$

$$[K] = B_e H_e \begin{bmatrix} \frac{7E_{11}}{3L_e} & \frac{7E_{13}}{3L_e} & \frac{E_{13}}{2} & \frac{-8E_{11}}{3L_e} & \frac{-8E_{13}}{3L_e} & \frac{2E_{13}}{3} & \frac{E_{11}}{3L_e} & \frac{E_{13}}{3L_e} & \frac{-E_{13}}{6} \\ \frac{7E_{13}}{3L_e} & \frac{7E_{33}}{3L_e} & \frac{E_{33}}{2} & \frac{-8E_{13}}{3} & \frac{-8E_{33}}{3L_e} & \frac{2E_{33}}{3} & \frac{E_{13}}{3L_e} & \frac{E_{33}}{3L_e} & \frac{-E_{33}}{6} \\ \frac{E_{13}}{2} & \frac{E_{33}}{2} & \frac{7E_{11}H_e^2}{36}+\frac{E_{33}L_e}{9} & \frac{-2E_{13}}{3} & \frac{-2E_{33}}{3} & \frac{-2E_{11}H_e^2}{9L_e}+\frac{E_{33}L_e}{9} & \frac{E_{13}}{6} & \frac{E_{33}}{6} & \frac{E_{11}H_e^2}{36}-\frac{E_{33}L_e}{18} \\ \frac{-8E_{11}}{3L_e} & \frac{-8E_{13}}{3L_e} & \frac{-2E_{13}}{3} & \frac{16E_{11}}{3L_e} & \frac{16E_{13}}{3L_e} & 0 & \frac{-8E_{11}}{3L_e} & \frac{-8E_{13}}{3L_e} & \frac{2E_{13}}{3} \\ \frac{-8E_{13}}{3L_e} & \frac{-8E_{33}}{3L_e} & -\frac{2E_{33}}{3} & \frac{16E_{13}}{3L_e} & \frac{16E_{33}}{3L_e} & 0 & \frac{-8E_{13}}{3L_e} & \frac{-8E_{33}}{3L_e} & \frac{2E_{33}}{3} \\ \frac{2E_{11}}{3} & \frac{2E_{33}}{3} & \frac{-2E_{11}H_e^2}{9L_e}+\frac{E_{33}L_e}{9} & 0 & 0 & \frac{4E_{11}H_e^2}{9L_e}+\frac{4E_{33}L_e}{9} & \frac{-2E_{13}}{3} & \frac{-2E_{33}}{3} & \frac{-2E_{11}H_e^2}{9L_e}+\frac{E_{33}L_e}{9} \\ \frac{E_{11}}{3} & \frac{E_{13}}{3L_e} & \frac{E_{13}}{6} & \frac{-8E_{11}}{3L_e} & \frac{-8E_{13}}{3L_e} & \frac{-2E_{13}}{3} & \frac{7E_{11}}{3L_e} & \frac{7E_{13}}{3L_e} & \frac{-E_{13}}{2} \\ \frac{E_{13}}{3L_e} & \frac{E_{33}}{3L_e} & \frac{E_{33}}{6} & \frac{-8E_{13}}{3L_e} & \frac{-8E_{33}}{3L_e} & \frac{2E_{33}}{3} & \frac{7E_{13}}{3L_e} & \frac{7E_{33}}{3L_e} & \frac{-E_{33}}{2} \\ \frac{-E_{13}}{6} & \frac{-E_{33}}{6} & \frac{E_{11}H_e^2}{36}-\frac{E_{33}L_e}{18} & \frac{2E_{13}}{3} & \frac{2E_{33}}{3} & \frac{-2E_{11}H_e^2}{9L_e}+\frac{E_{33}L_e}{9} & \frac{-E_{13}}{2} & \frac{-E_{33}}{2} & \frac{7E_{11}H_e^2}{36L_e}-\frac{E_{33}L_e}{18} \end{bmatrix} \quad (11)$$

Where, ρ_c: density of element

$$E_{11} = \bar{E}_{11}m^4 + 2(\bar{E}_{11} + 2\bar{E}_{33})m^2n^2 + \bar{E}_{22}n^4$$
$$E_{13} = (\bar{E}_{11} - \bar{E}_{12} + 2\bar{E}_{33})m^3n + (\bar{E}_{12} - \bar{E}_{22} + 2\bar{E}_{33})mn^3$$
$$E_{33} = (\bar{E}_{11} - 2\bar{E}_{12} + 2\bar{E}_{22})m^3n^2 + \bar{E}_{33}(m^4 + n^4)$$
$$\bar{E}_{11} = \frac{E_{xx}}{1 - v_{xy}^2\frac{E_{yy}}{E_{xx}}}$$
$$\bar{E}_{22} = \bar{E}_{11}; \quad \bar{E}_{12} = v_{xy}E_{22} \quad \text{and} \quad \bar{E}_{33} = G_{xy},$$
$$m = \cos\theta\,,\ n = \sin\theta$$

The modified effective stiffness matrices for the cracked GFLCB is obtained from the amplitudes of linear and transverse vibration of the GFLCB. The linear and transverse amplitudes of vibration ($\overline{U_i}$, $\overline{V_i}$) of ith cracked beam segment following the formulation for a single cracked beam (Krawzuk and Ostachowicz 1995, Dash 2013) is given by

$$\overline{U_i}(\overline{x}, t) = A_{2i-1}\ cos(\overline{K_U}\overline{x}) + A_{2i}\ sin(\overline{K_U}\overline{x}) \quad (12)$$

$$\overline{V_i}(\overline{x}, t) = B_{2j-1}\cos h\left(\overline{K_v}\overline{x}\right) + B_{2j}\ sinh(\overline{K_v}\overline{x}) + B_{2j+1}\cos(\overline{K_v}\overline{x}) + B_{2j+2}\ sin(\overline{K_v}\overline{x}) \quad (13)$$

With

$$i = 1{:}n \quad \text{and} \quad j = 2 \times i - 1$$
$$\overline{U_i} = \frac{U_i}{L_i}, \quad \overline{x} = \frac{L_{i+1} - L_i}{L},$$
$$\overline{V_i} = \frac{V_i}{L_i}, \quad \left(\overline{K_U}\right)_i = \frac{\varpi L_i}{(C_U)_i}$$
$$\left(\overline{K_V}\right)_i = \left(\frac{\varpi {L_i}^2}{(C_V)_i}\right)^{1/2}, \quad (C_U)_i = \left(\frac{E_c}{\rho_c}\right)^{1/2},$$
$$(C_V)_i = \left(\frac{E_c(I_c)_i}{A_i\rho_C}\right)^{1/2}$$

where 'E_c' and 'ρ_c' denotes Elastic modulus and density of the GFLCB determined from mixture rules of composites (Parida *et al*. 2022); $I = \frac{WH^3}{12}$, moment of inertia of intact beam and $(I_c)_i$ is moment inertia of i[th] cracked beam segment expressed by

$$(I_c)_i = 0.672\,z^2 - 1.04533\,z^3 + 4.5948z^4 - 9.973\,z^5 + 20.2948\,z^6 - 33.035z^7 + 47.106z^8 - 40.755\,z^9 + 19.6z^{10} \quad (14)$$

With $z = \frac{a_i}{H};\ i = 1{:}n.$

3. Finite element model

The differential equation of motion is (Khiem and Lien 2001)

$$X''''(x) - \lambda^4 X(x) = 0 \quad (15)$$

With

$$X''''(x) = K_1(\lambda\bar{x})\,Z_{j-1,1}^{+} + \frac{K_2(\lambda\bar{x})}{\lambda}Z_{j-1,2}^{+} + \frac{K_4(\lambda\bar{x})}{E_cI\lambda^3}Z_{j-1,3}^{+} - \frac{K_3(\lambda\bar{x})}{E_cI\lambda^2}Z_{j-1,4}^{+} \quad (16)$$

With

$$K_1(x) = \frac{1}{2}(cosh\,x + cos\,x),$$
$$K_2(x) = \frac{1}{2}(sinh\,x + sin\,x),$$
$$K_3(x) = \frac{1}{2}(cosh\,x - cos\,x),$$
$$K_4(x) = \frac{1}{2}(sinh\,x - sin\,x),$$
$$\lambda = \sqrt[4]{\omega^2\rho_C A/E_C I}$$

Z_j^+, Z_j^- are called state or position vector given by;

$Z_j^+ = J_j Z_j^-$; J_j: Jacobian matrix for the crack and is given by

$$J_j(\alpha) = \begin{bmatrix} 1 & 0 & 0 & 0 \\ 0 & 1 & 1 & \alpha \\ 0 & 0 & -1 & 0 \\ 0 & 0 & 0 & -1 \end{bmatrix}$$

$$Z_{ij}^{-} = K_1(\lambda l_j)Z_{j-1,1}^{+} + \frac{K_2(\lambda l_j)}{\lambda}Z_{j-1,2}^{+} + \frac{K_4(\lambda l_j)}{E_c I\lambda}Z_{j-1,3}^{+} - \frac{K_3(\lambda l_j)}{E_c I\lambda}Z_{j-1,4}^{+}$$

$$Z_{j2}^{-} = \lambda K_4(\lambda l_j)Z_{j-1,1}^{+} + +K_1(\lambda l_j)Z_{j-1,2}^{+} + \frac{K_3(\lambda l_j)}{\lambda}Z_{j-1,3}^{+} - \frac{K_2(\lambda l_j)}{E_c I\lambda}Z_{j-1,4}^{+}$$

$$Z_{j3}^{-} = -\lambda^3 E_C I K_2(\lambda l_j)Z_{j-1,1}^{+} - \lambda^2 E_C I K_3(\lambda l_j)Z_{j-1,2}^{+} - K_1(\lambda l_j)Z_{j-1,2}^{+} + \lambda K_4(\lambda l_j)Z_{j-1,2}^{+}$$

$$Z_{j4}^{-} = \lambda^2 E_C I K_3(\lambda l_j)Z_{j-1,1}^{+} + \lambda E_C I K_4(\lambda l_j)Z_{j-1,2}^{+} + \frac{K_2(\lambda l_j)}{\lambda}Z_{j-1,3}^{+} - K_1(\lambda l_j)Z_{j-1,4}^{+}$$

In general, above equations can be written as

$$\bar{Z}_j^{-} = T\bar{Z}_{j-1}^{+} \tag{17}$$

Where

$$l_j = x_j - x_{j-1}, \quad j = 1,2,3,\dots\ n$$

And

$$T_j(\lambda, l) = \begin{bmatrix} K_1(\lambda l) & \lambda^{-1}K_2(\lambda l) & \frac{K_4(\lambda l)}{E_C I\lambda^3} & \frac{-K_3(\lambda l}{E_C I\lambda^2}) \\ \lambda K_4(\lambda l) & K_1(\lambda l) & \frac{K_3(\lambda l}{E_C I\lambda^2} & \frac{-K_2(\lambda l)}{E_C I\lambda} \\ -\lambda^3 E_C I K_2(\lambda l) & -\lambda^2 E_C I K_3(\lambda l) & -K_1(\lambda l) & \lambda K_4(\lambda l) \\ \lambda^2 E_C I K_3(\lambda l) & \lambda E_C I K_4(\lambda l) & \lambda^{-1}K_2(\lambda l) & -K_1(\lambda l) \end{bmatrix}$$

The frequency function for a cantilever beam with 'n' number of cracks is

$$f(\lambda) = D_0 + D_{11}\alpha_L + D_{12}\beta_L + D_{13}\alpha_0 + D_{14}\beta_0 + D_{21}\alpha_L\beta_L + D_{22}\alpha_0\beta_0 + D_{23}\alpha_0\alpha_L + D_{24}\alpha_0\beta_L + D_{25}\alpha_L\beta_0 + D_{26}\beta_0\beta_L + D_{31}\alpha_0\alpha_L\beta_L + D_{32}\alpha_0\alpha_L\beta_0 + D_{33}\alpha_0\beta_0\beta_L + D_{34}\beta_0\alpha_L\beta_L + D_{44}\alpha\alpha_L\beta_0\beta_L = 0 \tag{18}$$

Where

$$D_0 = Q_{13}Q_{24} - Q_{14}Q_{23}, \quad D_{11} = Q_{13}Q_{44} - Q_{14}Q_{43},$$
$$D_{12} = Q_{24}Q_{33} - Q_{33}Q_{34} \quad D_{13} = Q_{12}Q_{23} - Q_{13}Q_{22},$$
$$D_{21} = Q_{44}Q_{33} - Q_{43}Q_{34}, \quad D_{22} = Q_{11}Q_{22} - Q_{21}Q_{12},$$
$$D_{23} = Q_{12}Q_{43} - Q_{13}Q_{42}, \quad D_{24} = Q_{13}Q_{24} - Q_{14}Q_{23},$$
$$D_{25} = Q_{14}Q_{41} - Q_{11}Q_{44}, \quad D_{26} = Q_{21}Q_{34} - Q_{24}Q_{31},$$
$$D_{31} = Q_{32}Q_{43} - Q_{42}Q_{23}, \quad D_{32} = Q_{11}Q_{42} - Q_{12}Q_{41},$$
$$D_{33} = Q_{11}Q_{42} - Q_{12}Q_{41}, \quad D_{44} = Q_{31}Q_{42} - Q_{41}Q_{32}$$

And

$$\alpha_0 = \frac{E_C I}{k_{OR}}, \quad \beta_0 = \frac{E_C I}{k_{OA}}, \quad \alpha_L = \frac{E_C I}{k_{LR}}, \quad \beta_L = \frac{E_C I}{k_{LA}}$$

k_{OR}, k_{OA}, k_{LR}, k_{LA} are the rotational and transverse spring stiffness at the left and right ends of the cantilever.

The elemental stiffness matrix of the crack beam can be obtained from the inverse of a modified flexible co-efficient matrix (Dash 2013)

$$Q_{crf} = [T]^t[C^{'}][T] \tag{19}$$

where

$$C^{'} = C_I + C_D \tag{20}$$

With

$$[C_I]^{-1} = [K_e]$$

For a cantilever beam with 'n' number of cracks and 'n+1' number of beam segments, the damage co-efficient matrix is given by

$$C_D = \begin{bmatrix} C_{1,1} & C_{1,2} & \cdots & C_{1,n+1} \\ C_{2,1} & C_{2,2} & \cdots & C_{2,n+1} \\ \vdots & \vdots & \vdots & \vdots \\ C_{n+1,1} & C_{n+1,2} & \cdots & C_{n+1,n+1} \end{bmatrix}$$

4. Hybrid AI model

The use of hybrid computational approaches such as RNN, Fuzzy-Logic, and mPSO improves the visibility and evaluation of the damage detection in structures. In this work, RNN, Fuzzy-Logic and mPSO are combined to optimize the result. The architecture of the individual AI methods is discussed below.

4.1 Recurrent Neural Network (RNNs)

RNNs are networks with extra memory where the previous step's output data are stored and inputted into the current phase that is needed to recognize crack locations and severity in a sequential pattern in the analogy. This structure of RNN is shown in Fig. 2 allows to study the temporal dynamic behavior in a time series.

The functional formula for the calculation of designed output parameter (y_t) is given in relation to previous state activation function (h_{t-1}), input(x_t) and the respective weights of recurrent neurons assigned to input activation function and to the output (W_{hh}, W_{xh}, W_{hy}) (Mohamad *et al*. 2009) as follows

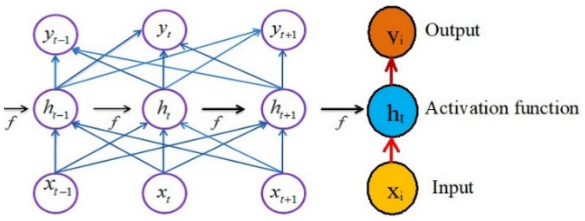

Fig. 2 The architecture of Recurrent Neural Network

$$h_t = f(h_{t-1}, x_t) \tag{21}$$

$$x_t = tanh(W_{hh}h_{t-1} + W_{xh}x_t) \tag{22}$$

$$y_t = W_{hy}h_t \tag{23}$$

Where h_t, h_{t-1}, h_{t+1}: activation function of current, Previous, and output states; x_t: input states, W_{hh}, W_{xh}, W_{hy}: weight of a recurrent neuron, input neuron, activation function and the output; y_t: Output states.

4.2 Fuzzy interference system (FIS) algorithm

Zadeh (2015) introduced fuzzy set theory in 1965. When dealing with imprecise and enigmatic data, it is possible to make definite decisions using fuzzy-logic. It can have a range of values between 0 and 1, instead of only true or false in fuzzy-logic. In this study, a hybrid form of the RNN-fuzzy-interference system used is a modification of the regular FIS. Each function in this combined structure contains a feedback connection that remembers prior information to construct sequential links. It improves the program's capacity to handle uncertainty and imprecision of parameters and the self-learning capability of the network. The RNN-Fuzzy interference system architecture shown in Fig. 3 has six levels. Fig. 3 shows the RNN-FIS architecture used in this work with 'n' time series inputs $\chi_1(a)$, $\chi_2(a)$ and $\chi_n(a)$ as the first three natural frequencies and one output $y(a)$. The structure of the RNN-FIS model was set for three layered models which have input, output, and hidden layer with six levels. The hidden layer uses the activation function (tanh) for the prediction of crack parameters in RNN, (Jena and Parhi 2020, Prakaash and Sivakumar 2020, Jena *et al*. 2017).

The first level indicates the input values represented as an 'n' dimensional vector with 'n' input nodes.

$$S_i^1(a) = \chi_i^1(a) \qquad i = 1,2,3, \dots, n \tag{24}$$

The Second level describes a fuzzification layer of the RNN-Fuzzy-interference system that uses stochastic class labels to translate input variables into fuzzy sets (Alazzawi and Wang 2021, Gomes *et al*. 2019).

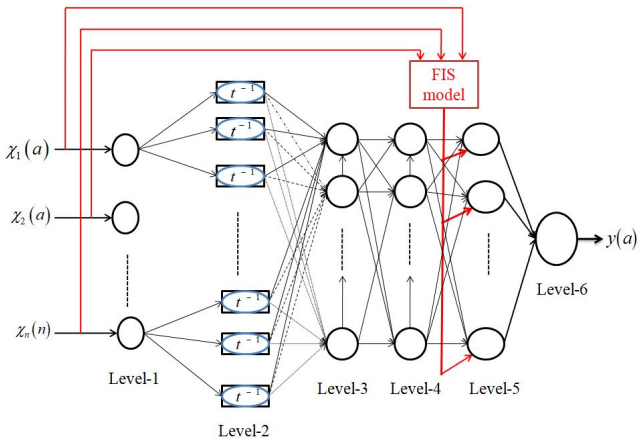

Fig. 3 The architecture of the RNN-Fuzzy interference system

$$S_{ij}^1(a) = exp\left\{-\frac{f_{ij}^1(a) - g_{ij}(a)}{\sigma_{ij}(a)}\right\} \qquad j = 1,2, \dots, m \tag{25}$$

Where $g_{ij}(a)$, $\sigma_{ij}(a)$ are the middle point and standard deviation of the j[th] Gaussian of the i[th] input.

$f_{ij}^1(a)$: input with recurrent connections as.

$$f_{ij}^2(a) = S_i^1(a) + S_{ij}^w(a) \tag{26}$$

Where

$$S_{ij}^w(a) = \omega_{ij}(a)S_{ij}^2(a) \qquad \omega_{ij}(a): \text{feedback weight.} \tag{27}$$

The third level shows the logic level, which creates the fuzzy set theory of each input parameter to perform the algorithm. The nodes in this level contain fuzzy rules, and the outputs use a fuzzy-interference system operation to calculate the "activation level" of the associated rule. The fourth level refers to the normalization level, which causes the rule of each node in the third level to conduct normalizing. The normalizing function in this level is given by

$$S_{nor}^4(a) = \frac{S_n^3(a)}{\sum_{nor=1}^{m^n} S_n^3(a)} \qquad nor = 1,2, \dots, m^n \tag{28}$$

m^n: number of normalizing nodes in the third level.

The fifth level is the final inference layer, which combines with the normalized constraints from the fourth level by the fuzzy-interference-system.

$$S_{nor}^5(a) = S_{nor}^4(a)F_{nor}(a) \tag{29}$$

$F_{nor}(a)$: fuzzy-interference-system model considering linear combinations of the system's current inputs and a constant.

The sixth level is the output level that recapitulates each output from the fifth level given by

$$S_{nor}^5(a) = S_{nor}^4(a)F_{nor}(a) \tag{30}$$

4.3 Modified Particle Swarm Optimization (mPSO)

PSO is a population-based, fabrication evolutionary optimization (Kennedy and Eberhart 1995) that optimizes the particle location using swarm intelligence. Initially, the positions and velocities of each particle within the search space are determined randomly. Each iteration updates the particle's location and velocity based on three variables for each particle are;

(i) The best position (p_{best} :P(x))
(ii) The best global position (g_{best}: G(x))
(iii) The best local position (l_{best}: L(x))

The following equations are used to perform each iteration of basic PSO

$$A(x+1) = A(x) + V(x+1) \tag{31}$$

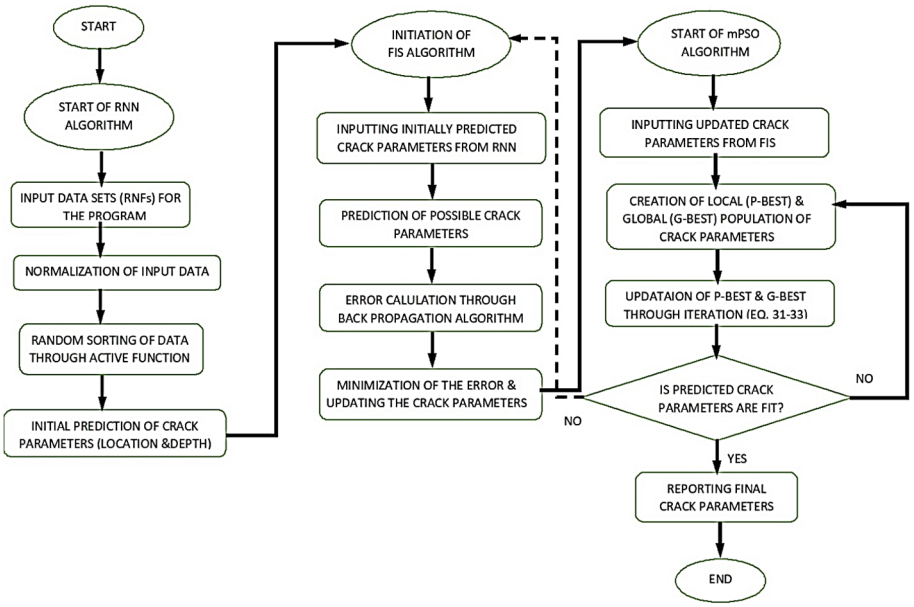

Fig. 4 The flowchart of the proposed hybrid AI model

$$v_i(x) = wv_i(x-1) + \rho_1\left(A_{pbest_i} - a_i(x)\right) + \rho_2\left(A_{pbest_i} - a_i(x)\right) \quad (32)$$

$$a_i(x) = a_i(x-1) + v_i(x) \quad (33)$$

Where, $V(x+1)$: Updated velocity, $A(x+1)$: Updated position.

4.4 RNN-FIS-mPSO algorithm

The proposed hybrid RNN-FIS-mPSO offers better performance with low mean square error (MSE)and faster adaptation capabilities to optimize the detection of damage parameters (crack location and depth) in GFLCB. The RNFs are first normalized and then sorted randomly in RNN. The initial crack location and depth are determined by RNN and fed as the input parameters to FIS. FIS minimizes the MSE through back propagation and updates the detected crack parameters. Further, these updated crack parameters are fed as the sampling data to generate the population of crack parameters in mPSO that locates the best possible crack parameters through certain iterations using the governing Eqs. (31)-(33) called membership function. Each membership function has three main parameters trained in the RNN-Fuzzy interference previously denotes each particle position that is adjusted by mPSO such that the resulting MSE has a minimized impact. Once the targeted level is achieved, the iteration is completed and the crack parameters are updated. For non-attaining the desired output level of crack parameters, the iteration is started again either from FIS input or from the mPSO iteration. The architecture of the proposed hybrid AI algorithm is shown in Fig. 4.

5. Validation

The credibility of the proposed model (RNN-FUZZY-PSO) is verified by a comparative study with the other AI model (MPSO) available in the literature. A GFLCB is taken and the first three RNFs are calculated using FEA. The material properties for the GFLCB are calculated using rule of mixture from the material property of the ingredient materials as presented in Table 2. The beam is assumed to have two cracks at two different locations two different crack severities. The three RNFs (RNFN, RSFN, and RTFN) are obtained from FEA and is used as input Parameters to train the algorithm. A set of twelve data sets are used for this purpose to identify the corresponding damage locations and severities. The computed location and severities of the damage are presented in Table 1. The comparison of the crack locations and severities by the present methodology (RNN-Fuzzy-PSO) is obtained from the inputted train data. Further, the superiority of the current method is observed over the referred observation by different crack detection methods such as mPSO (Jena *et al*. 2017), RNN **(**Jena and Parhi 2020) and RNN-mPSO **(**Nguyen *et al*. 2020) from the available RNFs. Error in calculation in crack depth (first and second) and locations (first and second) from the referred data sets of 12 location by the different methods with respect to FEA are calculated and presented in Figs. 5(a)-(d). The maximum error percentage in calculation of first crack location in a GFLCB by RNN-FUZZY-PSO, mPSO, RNN, and RNN-mPSO is found to be 3.08%, 5%, 7.2%, and 8.11% respectively. While for second crack depth the error percentage is 2.8%, 4.9%, and 6.1% by RNN-FUZZY-PSO, RNN, and RNN-mPSO. Similarly in detection of crack locations, the error percentage is found to be 1.1%, 5%, 7.2%, and 8.11%, for first crack by RNN-FUZZY-PSO, mPSO, RNN, and RNN-mPSO and 1.05%, 5.9%, and 6% by RNN-FUZZY-PSO, RNN, and RNN-mPSO for second crack respectively. It is observed the mean square error (MSE) in detecting the

severities of first crack and second crack is 0.013646245 and 0.008046635, While MSE in detection of crack location by the current method is 0.006804533, and 0.025366924 proving the superiority over other. The comparison of MSE in calculation of crack severities and locations by different methods are presented in Fig. 5(e).

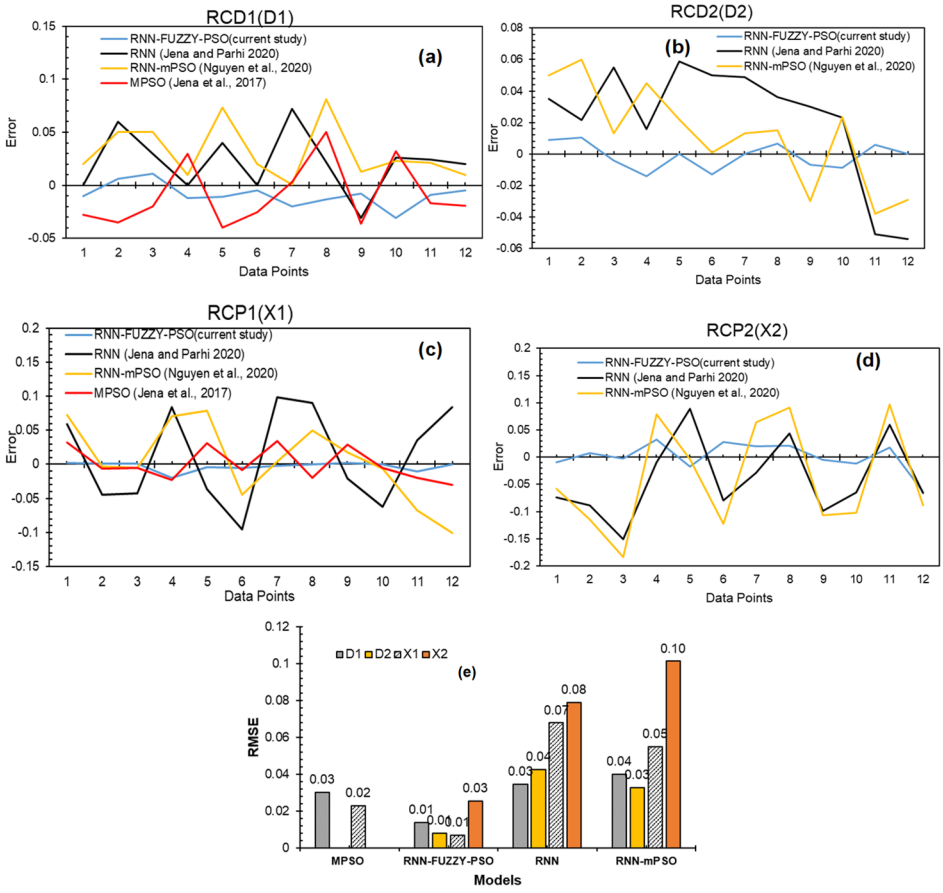

Fig. 5 Comparison of different models: (a) RCD at first crack position; (b) RCD at second crack position; (c) RCP of first crack; (c) RCP of second crack; (e) RMSE of different methods

Table 1 Validation of RNN-FUZZY-PSO model

Comparison of RCDs													
Sl. No.	RNFN	RSFN	RTFN	TRAIN DATA		TEST DATA (RNN-FUZZY-PSO) (current study)		mPSO (Jena *et al.* 2017)		RNN (Jena and Parhi 2020)		RNN-mPSO (Nguyen *et al.*, 2020)	
				D1	D2	D1	D2	D1	D2	D1	D2	D1	D2
1	0.942	0.944	0.97	0.300	0.300	0.310	0.291	0.328		0.300	0.265	0.280	0.250
2	0.990	0.999	0.992	0.400	0.300	0.394	0.290	0.435		0.340	0.278	0.350	0.240
3	1.000	0.997	0.993	0.300	0.300	0.289	0.304	0.320		0.270	0.245	0.250	0.287
4	0.944	0.939	0.939	0.400	0.416	0.412	0.430	0.370		0.400	0.400	0.390	0.371
5	0.999	0.993	1.000	0.300	0.300	0.311	0.300	0.340		0.260	0.241	0.227	0.278
6	0.995	0.999	0.996	0.300	0.300	0.305	0.313	0.325		0.300	0.250	0.280	0.299
7	0.997	0.987	1.000	0.400	0.300	0.420	0.300	0.397		0.328	0.251	0.399	0.287
8	0.932	0.937	0.969	0.400	0.436	0.413	0.430	0.350		0.378	0.400	0.319	0.421
9	1.000	0.995	0.987	0.400	0.300	0.408	0.307	0.436		0.431	0.270	0.387	0.330
10	0.949	0.946	0.943	0.300	0.263	0.331	0.272	0.268		0.274	0.240	0.277	0.239
11	0.951	0.950	0.948	0.200	0.222	0.209	0.216	0.217		0.176	0.273	0.179	0.260
12	0.948	0.953	0.966	-	-	0.205	0.300	0.219		0.180	0.354	0.190	0.329

Table 1 Continued

Comparison of RCPs													
Sl. No.	RNFN	RSFN	RTFN	TRAIN DATA		TEST DATA							
						RNN-FUZZY-PSO (current study)		MPSO (Jena *et al.* 2017)		RNN (Jena and Parhi 2020)		mPSO (Nguyen *et al.* 2020)	
				X1	X2	X1	X2	X1	X2	X1	X2	X1	X2
1	0.942	0.944	0.97	0.375	0.352	0.373	0.361	0.343		0.316	0.426	0.300	0.410
2	0.990	0.999	0.992	0.063	0.038	0.062	0.030	0.069		0.108	0.126	0.065	0.153
3	1.000	0.997	0.993	0.063	0.115	0.062	0.117	0.068		0.106	0.266	0.068	0.299
4	0.944	0.939	0.939	0.250	0.382	0.270	0.349	0.273		0.166	0.3916	0.200	0.303
5	0.999	0.993	1.000	0.375	0.395	0.379	0.412	0.344		0.411	0.306	0.300	0.399
6	0.995	0.999	0.996	0.250	0.277	0.255	0.249	0.258		0.345	0.356	0.300	0.399
7	0.997	0.987	1.000	0.750	0.639	0.752	0.619	0.716		0.651	0.667	0.748	0.575
8	0.932	0.937	0.969	0.750	0.57	0.750	0.549	0.770		0.660	0.526	0.700	0.479
9	1.000	0.995	0.987	0.375	0.437	0.373	0.441	0.346		0.396	0.536	0.355	0.544
10	0.949	0.946	0.943	0.063	0.097	0.063	0.109	0.068		0.125	0.162	0.069	0.199
11	0.951	0.950	0.948	0.500	0.627	0.510	0.609	0.520		0.465	0.567	0.577	0.530
12	0.948	0.953	0.966	0.500	-	0.498	0.564	0.530		0.416	0.566	0.599	0.589

6. Results and discussion

The present study is divided into two parts. In first part, the effect of presence of multiple cracks on the modal characteristics of cantilever GFLCB is presented. Multiple cracks at different crack locations as relative crack points (RCPs) and relative-crack-depths (RCD) are expressed and the corresponding changes in modal properties as function of relative natural frequencies (RNF) is presented using FEA. RCP, RCD, and RNF are expressed by

$$RCP_i = \frac{\text{Locationoftheith crack}}{\text{Length of the beam}},$$
$$\text{where } i = 1,2,3, \ldots,9$$
$$RCD_i = \frac{\text{Depth of ith crack}}{\text{Height of beam}},$$
$$\text{where } i = 1,2,3,\ldots,9$$
$$RNF = \frac{\text{Cracked beam natural frequency}}{\text{uncracked beam natural frequency}} = \frac{f_n^{'}}{f_n}$$

While modelling the cracked GFLCB cantilever, the mechanical and physical properties of as presented by Table 2 is used and the first three RNFs are determined using FEA. In the second part of work, the RNFs of GFLCB calculated by FEA are fed as the set of training data to RNN–fuzzy-mPSO algorithm to identify the crack positions and severities with minimum iteration time. In the second part of study, the effect of presence of multiple transverse cracks (upto nine cracks with equal RCD) are studied and also the integrity of the model to detect multiple cracks from the modal parameters are presented.

5.1 Effect of multiple cracks on beam dynamics

The effect of multiple cracks on the relative natural frequencies of the cantilever is studied. For this purpose, a few cracks in the cantilever GFLCB beam are modelled using FEA and the corresponding changes in RNFs are observed. In this study, the number of cracks gradually increased to nine. For a beam of one crack, the crack is modelled at the mid span of the beam, while for the two cracks, the cracks are placed at one third and two third of beam span respectively. Likewise, for nine cracks the beam is modelled to ten equally spaced blocks as mentioned in Fig. 1. The relative crack severity (RCSs) is taken to be constant while changing the crack numbers and corresponding changes in natural frequencies are observed. Further, the observations for different RCS values are calculated and presented by Table 3.

Table 2 Mechanical Properties and Dimension of GFLCB Materials (Sahoo and Jena 2021b, Parida and Jena 2023)

Entity (Unit)	Symbol	Value
Modulus of elasticity (GPa)	E_x	21.095
	E_y	21.095
	E_z	2.06
Modulus of rigidity (GPa)	G_{xy}	1.02
	G_{yz}	1.28
	G_{zx}	1.28
Density (Kg/m^3)	ρ	1855
Poisson's ratio	ν_{xy}	0.33
	ν_{yz}	0.39
	ν_{xz}	0.39
Length of beam (mm)	L	600
Width of beam (mm)	B	50
Thickness of beam (mm)	T	6

Table 3 Effect of multiple cracks on RNFs

No of Cracks	RCD	RFNF	RSNF	RTNF
1		0.9980	0.9968	0.9980
2		0.9972	0.9860	0.9910
3		0.9730	0.9830	0.9900
4		0.9750	0.9780	0.9880
5	**0.05**	0.9680	0.9760	0.9880
6		0.9630	0.9756	0.9830
7		0.9450	0.9753	0.9835
8		0.9380	0.9752	0.9830
9		0.9320	0.9750	0.9800
1		0.9820	0.9950	0.9920
2		0.9710	0.9780	0.9850
3		0.9510	0.9680	0.9805
4		0.9380	0.9650	0.9800
5	**0.1**	0.9310	0.9620	0.9795
6		0.9255	0.9610	0.9790
7		0.9150	0.9608	0.9780
8		0.9010	0.9608	0.9750
9		0.8985	0.9605	0.9650
1		0.9850	0.9870	0.9890
2		0.9450	0.9670	0.9750
3		0.9280	0.9540	0.9705
4		0.9130	0.9500	0.9705
5	**0.2**	0.8910	0.9480	0.9695
6		0.8810	0.9450	0.9690
7		0.8730	0.9430	0.9650
8		0.8610	0.9425	0.9610
9		0.8310	0.9422	0.9570
1		0.9750	0.9850	0.9750
2		0.9255	0.9550	0.9650
3		0.9015	0.9350	0.9616
4		0.8751	0.9305	0.9608
5	**0.3**	0.8520	0.9250	0.9605
6		0.8350	0.9240	0.9580
7		0.8250	0.9240	0.9550
8		0.8125	0.9235	0.9480
9		0.7850	0.9230	0.9350

It is observed that the natural frequency is reduced by the increase of number of cracks in the GFLCB cantilever as the flexibility increases. However, this drop of natural frequency is least observed in RSNF and RTNF as compared to RFNF. Fig. 6 presents variation of RNFs with the number of cracks present in a cantilever for the fixed RCS of 0.05. The variation of RNFs with RCSs for a cantilever with one crack at the mid-span of the beam is presented by Fig. 7(a). It is observed that increase of RCSs reduces the RNFs. However, the RFNF is reduced abruptly than that of RSNF and RTNF as presented by Figs. 7(b)-(d).

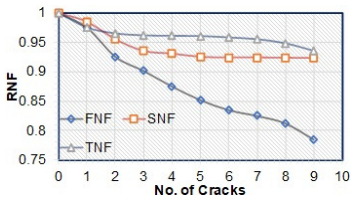

Fig. 6 Effect of multiple cracks on RNFs

It is because the relative changes in the fundamental mode are much higher than that of other RNFs. Also, it is evident that presence of multiple cracks induces much flexibility in the structure and as a result, RNFs are reduced.

5.2 Efficiency to detect crack parameters (RCP And RCS)

The proposed model predicts the presence of multiple cracks efficiently. In the proposed model, the three RNFs are used as input data to predict RCPs and RCSs. However, while predicting the RCPs of the current crack, the RCPs of previous cracks, the respective RCSs along with the RNFs are taken as input data. Fig. 8 presents the comparison of predicted locations (Output) with the actual crack locations (Target) in the GFLCB cantilever. It is observed that the error percentage while predicting the RCPs is within the minimum limit (2% maximum). Further, it is observed that the prediction probability of RCP is strongly dependent on RCSs as the stiffness of a structure is affected by the presence of cracks. The locations and severities of a beam with the multiple cracks are interdependent. In the proposed hybrid model, the algorithm works better for increased initial crack population. Hence it is observed, the prediction error percentage is minimum for predicting the crack locations for a beam with more number of cracks and minimum for beam with least number of cracks. Henceforth it is observed that the prediction probability of ninth crack location is very much more accurate than predicting the first crack position. From the study, the average error of prediction of RCPs for one to nine crack are found to be 1.86, 1.85, 1.63, 1.51, 1.35, 1.30, 1.28, 1.13, 1.05, and 0.84% respectively. Fig. 9 presents the mean error and the standard deviations of the proposed model while predicting the multiple crack location for a beam with nine cracks. The error min and standard deviation for the prediction of the ninth crack is almost negligible (1.5e-15), depicting the realness of the measurement. It is observed that like RCPs, the RCSs are also forecasted for the occurrences of multiple defects. Fig. 10 presents the comparison of actual RCSs (Target) and the Predicted RCSs (output) through the proposed model. The mean square error is observed to be much less (0.01154) with a mean error percentage of 1.3%.

6. Conclusions

In this study, a hybrid AI technique for the prediction of crack parameters from modal parameters is proposed. First, FEA is conducted to find the vibration parameters (fundamental frequency and mode shape) of multi-cracked

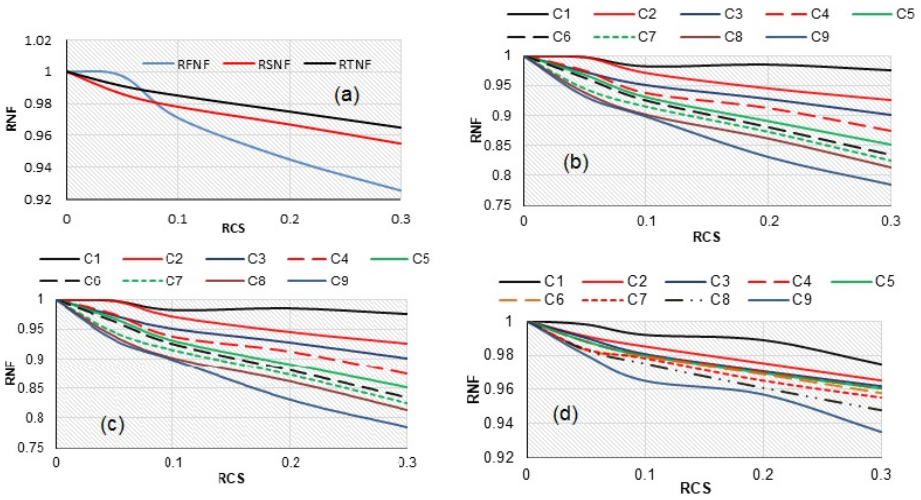

Fig. 7 Effect of RCS on RNFs: (a) RCS vs. RNF for a beam with one crack; (b) RFNF vs. RCS for multiple crack; (c) RSNF vs. RCS for multiple cracks; (d)RTNF vs. RCS for multiple cracks

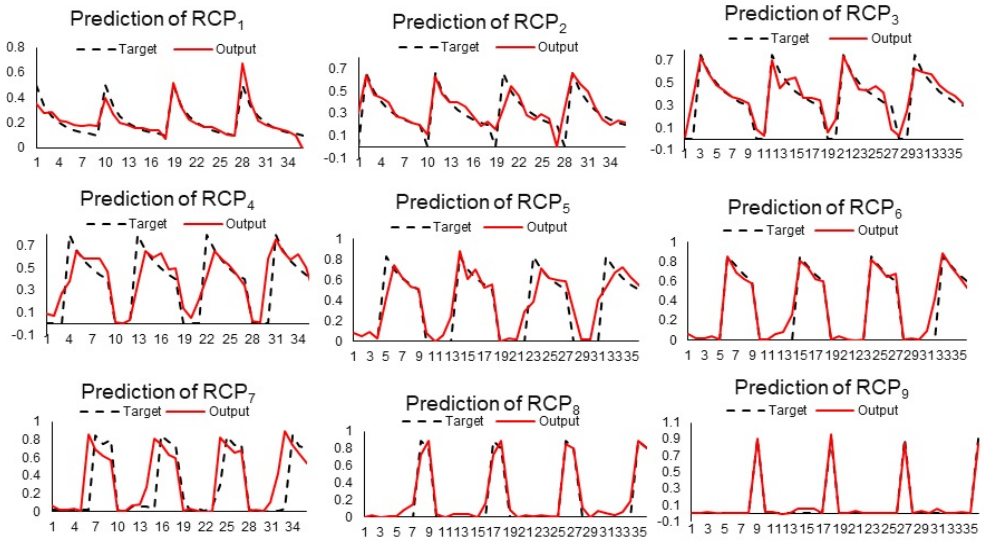

Fig. 8 Prediction of RCPs in beam with multiple crack

laminated composite beams (GFLCB) (considered nine transverse cracks at different locations and different sizes of crack severity) and the results are noted. Then, these results are used as a set of inputs to train the proposed AI-hybrid model (RNN-Fuzzy-mPSO) to forecast the crack location and severities. From the study, the following observations are made.

- It is observed that natural frequency is reduced by the increase in the number of cracks in the GFLCB cantilever as the flexibility increases. This drop in natural frequency is least observed in second and third relative natural frequencies (RSNF and RTNF) as compared to relative fundamental natural frequency (RFNF).
- In addition, it is observed that an increase of relative crack severities causes the loss of stiffness of the beam as the stress-affected zone is increased reducing the RNFs.
- The maximum error percentage in calculation of first crack location in a GFLCB by RNN-FUZZY-PSO, mPSO, RNN, and RNN-mPSO is found to be 3.08%, 5%, 7.2%, and 8.11% respectively. While for second crack depth the error percentage is 2.8%, 4.9%, and 6.1% by RNN-FUZZY-PSO, RNN, and RNN-mPSO.
- Similarly in detection of crack locations, the error percentage is found to be 1.1%, 5%, 7.2%, and 8.11%, for first crack by RNN-FUZZY-PSO, mPSO, RNN, and RNN-mPSO and 1.05%, 5.9%, and 6% by RNN-FUZZY-PSO, RNN, and RNN-mPSO for second crack respectively.

It is observed the mean square error (MSE) in detecting the severities of first crack and second crack is 0.013646245 and 0.008046635, While MSE in detection of crack location by the current method is 0.006804533, and 0.025366924 proving the superiority over other.

- The proposed RNN-Fuzzy-mPSO hybrid model is

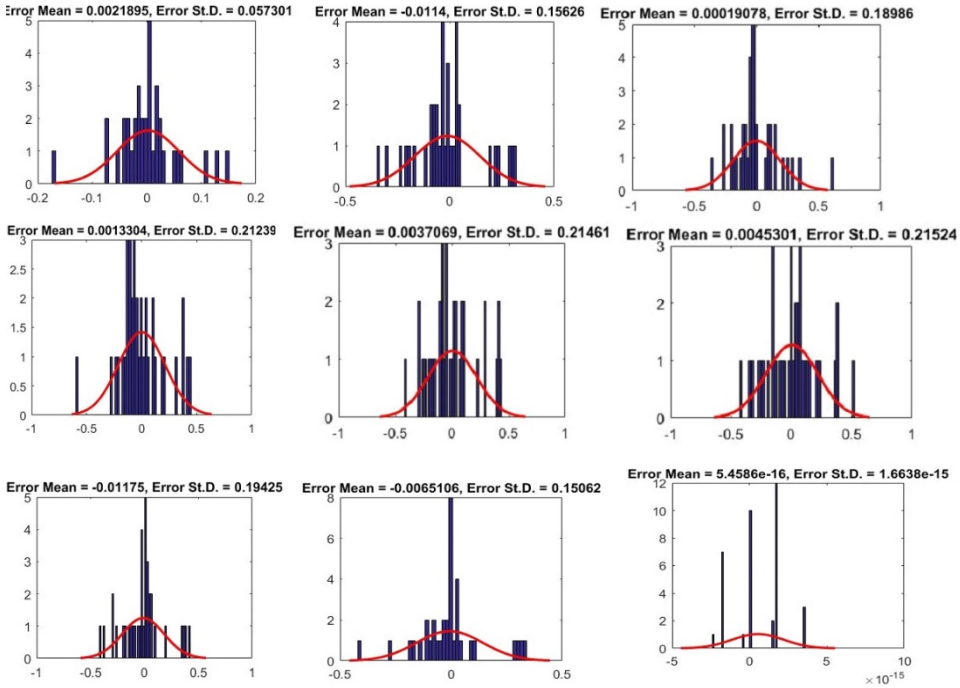

Fig. 9 Standard deviations of the proposed model

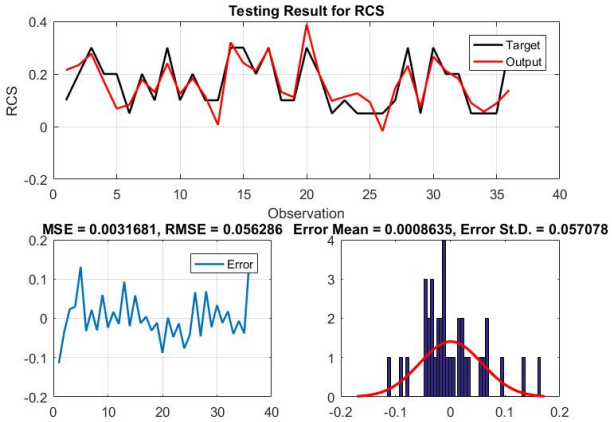

Fig. 10 Variation of RCS and MSE

effective for predicting the crack parameters of a GFLCB cracked beam. it is expected that the forecasted location and severity of the crack from actual ones will slightly differ with a mean error of 0.8% by this method. Further, it is observed that when a greater number of modal inputs are given to the algorithm, it trains the algorithm well and shows minimum error. Thus, the higher value of error in prediction inhibits scarce input data implicating not to be very useful in predicting the faults in structures of minimum modal input data sets.

- Though the mean error is near about 0.8%, the standard deviation of it is very negligible. Hence, it is an effective technique for predicting the multiple transverse crack positions and their severities in laminated composite structures.
- LHCBs can replace conventional composites due to the fact that, the properties are tailorable to the specific locations. Hence can have wide spread application in automobiles bodies, floating vessels and structural and furniture replacements of the modern buildings.
- The proposed hybrid AI method is an effective method of crack detection and can used to detect location of holes or cracks in composite structures used in automobiles bodies, floating vessels and structural and furniture replacements of the modern buildings from the vibration signatures using vibration analyzer.

Acknowledgments

The authors do here acknowledge the research facilities available in VSSUT, Burla.

Research funding

Authors declare that there is no funding received to carry out this research work.

Conflict of interest

Authors have no conflict of interest.

Ethical approval

This manuscript is original research, and it is not submitted elsewhere.

Author's contribution

Saritprava Sahoo, Sarada Prasad Parida, and Pankaj Charan Jena contributed to the study's conception and design. Material preparation is done by Sarada Prasad Parida and Saritprava Sahoo. The theoretical formulation is conducted by Sarada Prasad Parida and Pankaj Charan Jena. Data collection was performed by Saritprava Sahoo. Pankaj Charan Jena performed the analysis. Saritprava Sahoo and Sarada Prasad Parida wrote the first draft of the manuscript, which was subsequently reviewed by Pankaj Charan Jena, and finalized manuscript. All authors read and approved the final manuscript.

References

Abdeljaber, O., Avci, O., Kiranyaz, S., Gabbouj, M. and Inman, D.J. (2017), "Real-time vibration-based structural damage detection using one-dimensional convolutional neural networks", *J. Sound Vib*., **388**(1), 154-170. https://doi.org/10.1016/j.jsv.2016.10.043

Alazzawi, O. and Wang, D. (2021), "Deep convolution neural network for damage identifications based on time-domain PZT impedance technique", *J. Mech. Sci. Technol*., **35**(5), 1809-1819. https://doi.org/10.1007/s12206-021-0401-y

Babu Rao, K. and Mallikarjuna Reddy, D. (2021), "Fault detection in rotor system by discrete wavelet neural network algorithm", *J Vib. Control*, **28**(21-22), 3315-3331. https://doi.org/10.1177/10775463211030754

Capozucca, R. and Magagnini, E. (2018), "Experimental vibration response of homogeneous beam models damaged by notches and strengthened by CFRP lamina", *Compos. Struct*., **206**, 563-577. https://doi.org/10.1016/j.compstruct.2018.08.082

Chandrashekhar, M. and Ganguli, R. (2009), "Damage assessment of structures with uncertainty by using mode- shape curvatures and fuzzy logic", *J. Sound Vib*., **326**(3-5), 939-957. https://doi.org/10.1155/2013/164853

Das, P., Muni, M.K. and Sahu, S.K. (2021), "On crack detection in a laminated glass/epoxy composite beam under free vibration with fuzzy logic aid", *Int. J. Struct. Stab. Dyn*., **21**(13), p. 2150176. https://doi.org/10.1142/S0219455421501765

Das, P., Muni, M.K., Pradhan, N., Basa, B. and Sahu, S.K. (2024), "Fuzzy logic for crack detection in cantilever-laminated composite beam using frequency response", *J. Braz. Soc. Mech. Sci. Eng*., **46**(4), p. 250. https://doi.org/10.1007/s40430-024-04829-7

Dash, A.K. (2013), "Analysis of adaptive fuzzy technique for multiple crack diagnosis of faulty beam using vibration signatures", *Adv. Fuzzy Syst*., pp. 1-16. https://doi.org/10.1155/2013/164853

Davim, J.P. (2017a), *Green Composites*: *Materials*, *Manufacturing and Engineering*, Berlin, Boston: De Gruyter. https://doi.org/10.1515/9783110435788.

Davim, J.P. Ed. (2017b), *Statistical and computational techniques in manufacturing*, Berlin, Heidelberg: Springer. https://doi.org/10.1007/978-3-642-25859-6

Davim, J.P., Rubio, J.C. and Abrao, A.M. (2007), "A novel approach based on digital image analysis to evaluate the delamination factor after drilling composite laminates", *Compos. Sci. Technol*., **67**(9), 1939-1945. https://doi.org/10.1016/j.compscitech.2006.10.009

Dos Santos, J.A., Soares, C.M., Soares, C.M. and Maia, N.M.M. (2005), "Structural damage identification in laminated structures using FRF data", *Compos. Struct*., **67**(2), 239-249. https://doi.org/10.1016/j.compstruct.2004.09.011

Duan, Z., Jung, Y., Yan, J. and Lee, I. (2020), "Reliability-based multi-scale design optimization of composite frames considering structural compliance and manufacturing constraints", *Struct. Multidiscip. Optim*., **61**, 2401-2421. https://doi.org/10.1007/s00158-020-02517-3

Ganguli, R. (2001), "A fuzzy logic system for ground based structural health monitoring of a helicopter rotor using modal data", *J. Intell. Mater. Syst. Struct*., **12**(6), 397-407. https://doi.org/10.1106/104538902022598

Gomes, G.F., De Almeida, F.A., Junqueira, D.M., da Cunha Jr, S.S. and Ancelotti Jr, A.C. (2019), "Optimized damage identification in CFRP plates by reduced mode shapes and GA-ANN methods", *Eng. Struct*., **181**, 111-123. https://doi.org/10.1016/j.engstruct.2018.11.081

Jang, R. (1993), "IS: Adaptive-Network-Based Fuzzy Inference System", *IEEE Trans. Syst. Man. Cybern*., **23**(3), 665-685. https://doi.org/10.1109/21.256541

Jena, P.K. and Parhi, D.R. (2015), "A modified particle swarm optimization technique for crack detection in cantilever beams", *Arab. J. Sci. Eng*., **40**(11), 3263-3272. https://doi.org/10.1007/s13369-015-1661-6

Jena, S.P. and Parhi, D.R. (2020), "Fault detection in cracked structures under moving load through a recurrent-neural-networks-based approach", *Scientia Iranica*, **27**(4), 1886-1896. https://doi: 10.24200/sci.2019.50363.1657

Jena, P.C., Pohit, G. and Parhi, D.R. (2017), "Fault measurement in composite structure by fuzzy-neuro hybrid technique from the natural frequency and fibre orientation", *J. Vib. Eng. Technol*., **5**(2), 123-136.

Kang, F., Li, J-j. and Xu, Q. (2012), "Damage detection based on improved particle swarm optimization using vibration data", *Appl. Soft Comput*., **12**(8), 2329-2335. https://doi.org/10.1016/j.asoc.2012.03.050

Khatir, S., Dekemele, K., Loccufier, M., Khatir, T. and Wahab, M.A. (2018), "Crack identification method in beam-like structures using changes in experimentally measured frequencies and Particle Swarm Optimization", *Comptes Rendus. Mécanique*, **346**(2), 110-120. https://doi.org/10.1016/j.crme.2017.11.008

Kaveh, A., Dadras, A. and Geran Malek, N. (2019), "Robust design optimization of laminated plates under uncertain bounded buckling loads", *Struct. Multidiscip. Optim*., **59**, 877-891. https://doi.org/10.1007/s00158-018-2106-0

Kennedy, J. and Eberhart, R. (1995), "Particle swarm optimization", *Proceedings of the IEEE International Conference on Neural Networks*, **4**, 1942-1948. https://doi.org/10.1109/ICNN.1995.488968

Khiem, N.T. and Lien, T.V. (2001), "A simplified method for natural frequency analysis of a multiple cracked beam", *J. Sound Vib*., **245**(4), 737-751. https://doi.org/10.1006/jsvi.2001.3585

Krawczuk, M. and Ostachowicz, W.M. (1995), "Modelling and vibration analysis of a cantilever composite beam with a transverse open crack", *J. Sound Vib*., **183**(1), 69-89. https://doi.org/10.1006/jsvi.1995.0239

Liu, J., Han, Z. and Hu, R. (2022), "Research of vibration and crack propagation controls on an asymmetrical cracked rotor", *J. Vib. Control*, **28**(13-14), 1686-1697. https://doi.org/10.1177/1077546321998221

Mohamad, M., Tokhi, M.O., Toha, S.F. and Latiff, I.A. (2009), "Particle swarm modelling of a flexible beam structure", *Third* In: *UK Sim European Symposium on Computer Modeling and Simulation*, pp. 31-36. https://doi.org/10.1109/EMS.2009.109

Naderpour, H. and Mirrashid, M. (2018), "Shear strength prediction of RC beams using adaptive neuro-fuzzy inference system", *Sci. Iran*, **27**(2), 657-670.

https://doi.org/10.24200/SCI.2018.50308.1624
Nguyen, Q.H., Ly, H.B., Le, T.T., Nguyen, T.A., Phan, V.H., Tran, V.Q. and Pham, B.T. (2020), "Parametric investigation of particle swarm optimization to improve the performance of the adaptive neuro-fuzzy inference system in determining the buckling capacity of circular opening steel beams", *Materials* (*Basel*), **13**(10), p. 2210. https://doi.org/10.3390/ma13102210
Nikkhoo, A., Karegar, H., Karami Mohammadi, R. and Hajirasouliha, I. (2021), "An acceleration-based approach for crack localisation in beams subjected to moving oscillators", *J. Vib. Control*, **27**(5-6), 489-501. https://doi.org/10.1177/1077546320929821
Nouri Shirazi, M.R., Mollamahmoudi, H. and Seyedpoor, S.M. (2014), "Structural damage identification using an adaptive multi-stage optimization method based on a modified particle swarm algorithm", *J. Optim. Theory Appl.*, **160**, 1009-1019. https://doi.org/10.1007/s10957-013-0316-6
Parida, S.P. and Jena, P.C. (2023), "Multi-fillers GFRP laminated composite plates: fabrication & properties", *Indian J. Eng. Mater. Sci.*, **29**(6), 817-825.
Parida, S.P., Jena, P.C. and Dash, R.R. (2022), "Dynamics of rectangular laminated composite plates with selective layer-wise fillering rested on elastic foundation using higher-order layer-wise theory", *J. Vib. Control*, **29**(23-24), 5598-5615. https://doi.org/10.1177/10775463221138353
Parida, S.P., Sahoo, S. and Jena, P.C. (2024), "Prediction of multiple transverse cracks in a composite beam using hybrid RNN-mPSO technique", *Proc. Inst. Mech. Eng. Part C*, **238**(16), 7977-7986. https://doi:10.1177/09544062241239415
Prakaash, A.S. and Sivakumar, K. (2020), "Optimized recurrent neural network with fuzzy classifier for data prediction using hybrid optimization algorithm: Scope towards diverse applications", *Int. J. Wavelets Multiresol. Inform. Process.*, **19**(02), p. 2050074. https://doi.org/10.1142/s0219691320500745
Rautela, M. and Gopalakrishnan, S. (2020), "Ultrasonic guided wave based structural damage detection and localization-using model assisted convolutional and recurrent neural networks", *Expert Syst.*, **167**, p. 114189. https://doi.org/10.1016/j.eswa.2020.114189
Sahoo, S. and Jena, P.C. (2021a), "Analysis of GFRP cracked cantilever beam using artificial neural network", *Mater. Today Proc.*, **44**(1), 1788-1793. https://doi.org/10.1016/j.matpr.2020.11.970
Sahoo, S. and Jena, P.C. (2021b), "Preparation and characterization of hybrid laminated composite beams", *Adv. Mater. Process. Tech.*, **8**(sup2), 899-912. https://doi.org/10.1080/2374068X.2021.1953924
Samir, K., Brahim, B., Capozucca, R. and Wahab, M.A. (2018), "Damage detection in CFRP composite beams based on vibration analysis using proper orthogonal decomposition method with radial basis functions and cuckoo search algorithm", *Compos. Struct.*, **187**, 344-353. https://doi.org/10.1016/j.compstruct.2017.12.058
Seitllari, A. and Naser, M.Z. (2019), "Leveraging artificial intelligence to assess explosive spalling in fire-exposed RC columns", *Comput. Concrete, Int. J.*, **24**(3), 271-282. https://doi.org/10.12989/cac.2019.24.3.271
Sepehry, N., Ehsani, M., Zhu, W. and Bakhtiari-Nejad, F. (2021), "Application of scaled boundary finite element method for vibration-based structural health monitoring of breathing cracks", *J. Vib. Control*, **27**(23-24), 2870-2886. https://doi.org/10.1177/1077546320968646
Seyedpoor, S.M. (2011), "Structural damage detection using a multi-stage particle swarm optimization", *Adv. Struct. Eng.*, **14**(3), 533-549. https://doi.org/10.1260/1369-4332.14.3.533
Sun, W., Yang, G., Chen, Q., Palazoglu, A. and Feng, K. (2013), "Fault diagnosis of rolling bearing based on wavelet transform and envelope spectrum correlation", *J. Vib. Control*, **19**(6), 924-941. https://doi.org/10.1177/1077546311435348
Thatoi, D., Choudhury, S. and Jena, P.K. (2014), "Fault diagnosis of beam-Like structure using modified fuzzy technique", *Adv. Acoust. Vib.*, **2014**(1), p. 491510. https://doi.org/10.1155/2014/491510
Tran-Ngoc, H., Khatir, S., De Roeck, G., Bui-Tien, T. and Wahab, M.A. (2019), "An efficient artificial neural network for damage detection in bridges and beam-like structures by improving training parameters using cuckoo search algorithm", *Eng. Struct.*, **199**, p. 109637. https://doi.org/10.1016/j.engstruct.2019.109637
Zadeh, L.A. (2015), "Fuzzy logic—a personal perspective", *Fuzzy sets syst.*, **281**, 4-20. https://doi.org/10.1016/j.fss.2015.05.009
Zang, C. and Imregun, M. (2001), "Combined neural network and reduced FRF techniques for slight damage detection using measured response data", *Arch. Appl. Mech.*, **71**(8), 525-536. https://doi.org/10.1007/s004190100154
Zhou, J., Li, Z. and Chen, J. (2018), "Damage identification method based on continuous wavelet transform and mode shapes for composite laminates with cutouts", *Compos. Struct.*, **191**(1), 12-23. https://doi.org/10.1016/j.compstruct.2018.02.02

Symbols used

L	length of beam
L_n	position of nth crack
W	width of beam
H	height of beam
a_n	crack depth of nth crack
ν	Poisson's ratio
E	modulus of elasticity
E_C	modulus of elasticity of the composite
E_{11}, E_{22}, E_{33}, E_{12}, E_{13}	modulus of elasticity of laminate along x-axis, y axis and z-axis, xy-plane and xz-plane
K_{In}	stress intensity factor for Mode-I fracture at nth crack location
K_{IIn}	stress intensity factor for mode-II fractures at nth crack location
m	total number of cracks
C_{ijn}	Flexibility co-efficient for nth crack
U_{ijn}	Strain energy due to nth crack
J_{cn}	strain energy release rate at nth crack location
P_1	axial load
P_2	bending moment
K_e	Element stiffness matrix
K_{cr}	stiffness matrix of cracked structure
K_{eff}	Equivalent effective stiffness of cracked beam
K_{Crn}	Stiffness of cracked beam
K_{Int}	Stiffness of intact beam
X_n	position of n^{th} crack
[M]	Mass matrix
$[M_e]$	Element mass matrix
ω	Natural frequency
U_i (i = 1, 6)	displacement of beam along X direction
V_j,(j = 1, 6)	displacement of beam along Y direction
RCP	relative crack position
RCS	relative crack Severity
L_e	length of element
H_e	Height of element
B_e	width of element
A	cross sectional area of beam
ρ	Density
ρ_c	Density of composite
I	Moment of inertia
K_e	effective elemental stiffness matrix of beam element in FEA
K_{crf}	crack elemental stiffness matrix
T	transformation matrix
C'	flexible co-efficient matrix
C_I	flexible co-efficient matrix of intact beam
C_D	flexible co-efficient matrix of cracked beam